ISSN 0030-400X, Optics and Spectroscopy, 2016, Vol. 121, No. 3, pp. 357–363. © Pleiades Publishing, Ltd., 2016.
Original Russian Text © A.S. Kasprzhitskii, G.I. Lazorenko, S.N. Sulavko, V.A. Yavna, A.G. Kochur, 2016, published in Optika i Spektroskopiya, 2016, Vol. 121, No. 3, pp. 387–394.

CONDENSED-MATTER SPECTROSCOPY

A Study of the Structural and Spectral Characteristics of Free and Bound Water in Kaolinite

A. S. Kasprzhitskii, G. I. Lazorenko, S. N. Sulavko, V. A. Yavna, and A. G. Kochur

Rostov State Transport University, Rostov-on-Don, 344038 Russia

e-mail: glazorenko@yandex.ru

Received March 14, 2016

Abstract—The dependence of the Si–O stretching vibration line intensity in the IR spectrum of kaolinite on the humidity of this mineral has been experimentally investigated. The experimental data were interpreted on the basis of density functional theory (DFT) calculations with allowance for the real crystallographic features of the kaolinite sample, determined by structural analysis. Some specific features of the intensity behavior in the plastic state are revealed, which can be used to develop techniques for determining its limits. The differences in the O–H bond lengths and H–O–H angles for the H_2O molecules adsorbed by basal surfaces and located in the porous space of the mineral are determined. Based on the DFT data, it was found that bond lengths and bond angles for a water molecule adsorbed on the siloxane surface are systematically smaller than for a water molecule adsorbed on the hydroxyl surface.

DOI: 10.1134/S0030400X16090113

INTRODUCTION

In recent years, researchers have paid much attention to the spatial and electronic structure of hydrated aluminosilicates in view of the good prospects of their application to solve various problems of science and technology. They are widely used as fillers of polymer nanocomposites [1], high-efficiency sorbents [2], catalysts [3], sensors [4], antibacterial materials [5], barriers for disposal and utilization of radioactive waste [6], and a raw material in the construction material industry [7].

The application of layered aluminosilicates in different fields of technology is related in many respects to the specific features of their hydration, which determines to a great extent their physicochemical properties. Despite the large number of studies on this subject, there is no unified point of view in understanding the mechanisms of interaction of layered aluminosilicates with materials in liquid-phase reactions, in defining the concept of "bound water," and in the questions of determining the plasticity and sorption properties of these objects [8].

Hence, a detailed study of these processes is of great theoretical and practical interest. The aforementioned concepts and the mechanisms determining the phenomenological properties can be refined by studying the processes of interaction of H_2O molecules with basal surfaces. The corresponding theoretical studies are generally performed using the density functional theory (DFT) method [9, 10], which proved to be good in calculations of the structural and vibrational characteristics, sorption, electrical, mechanical, and other physical properties of these objects [11–15].

Studies of recent years made it possible to refine the character of interaction of H_2O molecules with the adsorbing surfaces of aluminosilicates and the structural changes in the interacting atomic groups that occur during this process [16–19].

In this paper, we report the results of studying the influence of kaolinite hydration on the structural features of H_2O molecules located at basal surfaces and in the kaolinite porous space and on the relative intensities of IR lines of kaolinite at different levels of its humidity.

MATERIALS AND METHODS

Object of Study

The study was performed on kaolinite samples from the Glukhovetskoe deposit (Ukraine). The kaolinite crystal structure is known to contain two basic structural elements: (i) silicon–oxygen tetrahedra and (ii) octahedra consisting of oxygen atoms or hydroxyl groups, with octahedrally coordinated aluminum, magnesium, or iron atoms inside these polyhedra [20]. Sharing oxygen-containing vertices, these structural elements form two-dimensional hexagonal networks constructed from SiO_4 tetrahedra and AlO_6 octahedra.

An alignment of networks of tetrahedra and octahedra leads to the formation of two-level kaolinite packets (Fig. 1).

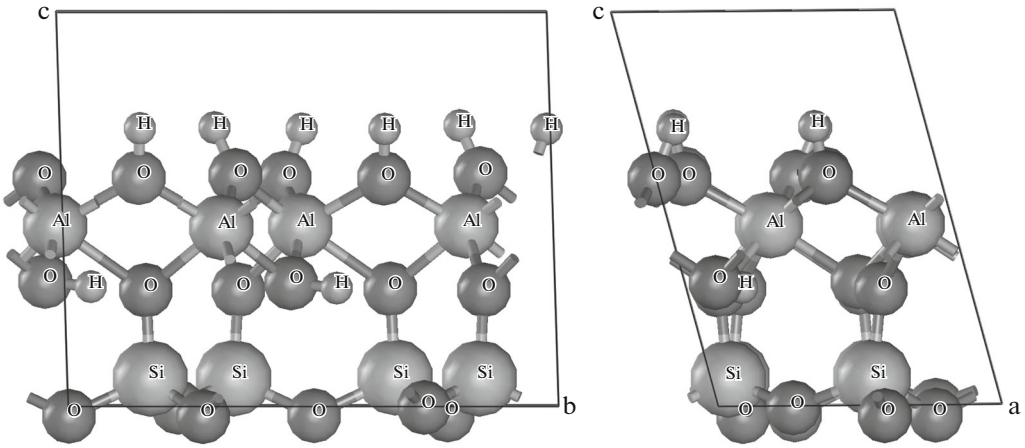

Fig. 1. Kaolinite unit cell.

In the experimental study of the IR spectra, the mineral samples were subjected to preliminary testing according to [21]]. A selected clay fraction with particle sizes in the range of 0.04–3.0 μm was monitored with a CPSDC24000 analyzer of fine-grained particles using centrifugal sedimentation in liquid [22]. The sizes of clay fraction particles of the kaolinite sample turned out to be mainly in the range of 0.2–0.8 μm; hence, the methods of frustrated total internal reflection can be used to obtain IR spectra of kaolinite in the dry and moistened states, because the light penetration depth into moistened/liquid samples is estimated to be 5–50 μm.

X-Ray Diffraction Study

An X-ray diffraction study of the clay fraction of kaolinite was performed using a Rigaku diffractometer at the Institute of Ore Geology, Petrography, Mineralogy, and Geochemistry, Russian Academy of Sciences (Moscow). The details of the experiment and methods of analysis were reported in [23].

The calculated structural parameters of kaolinite are listed in the table, along with the data of other researchers. A comparison of these data gives an idea about the variation in the lattice parameters of kaolinites from different deposits.

The data of [23] from the table were used as the initial approximation in the theoretical study of the spatial and electronic structure of the mineral and its IR spectra at different degrees of moistening.

IR Spectra of Kaolinite Samples with Different Humidities

We investigated kaolinite samples with different levels of humidity, which was specified by the mass ratio of H_2O and mineral in the sample:

$$w = m_{H_2O}/m_{clay}.$$

IR spectra were analyzed using an ALPHA IR Fourier spectrometer (ALPHA-E module, Bruker) by the method of frustrated total internal reflection. The spectra were recorded in the mid-IR range using the OPUS software (which enters the delivery set of the equipment). The native surface of the sample on a ZnSe crystal (with a contact area of 19.6 mm^2) was investigated. The spectrum for each humidity value was obtained by averaging over 25 scans; this approach made it possible to establish reliably the fine structure of the spectra at specified sample humidities and provide a resolution of 2 cm^{-1}.

Computer Simulation of the Atomic and Electronic Structures of Kaolinite

The electronic structure and properties of kaolinite were calculated by the DFT method, implemented in

Unit-cell parameters of kaolinite

Source	Lattice parameter, Å			Angle, deg			Unit-cell volume, $Å^3$
	a	*b*	*c*	α	β	γ	*V*
[23]	5.215	9.011	7.460	91.910	104.655	89.885	338.919
[24]	5.155	8.945	7.405	91.700	104.862	89.822	329.893
[25]	5.153	8.942	7.391	91.926	105.046	89.797	328.708

the CASTEP software, using the resources of the supercomputer complex at Moscow State University [26].

The surfaces of clay particles were modeled by surfaces of packets of infinitely large size along the directions of two axes and by one unit cell in the direction of the third axis. This model can be considered justified on the assumption of weak mutual influence of the adsorption events of H_2O molecules on hydroxyl and siloxane surfaces of kaolinite.

The Bloch functions of electrons in the mineral samples were determined in the form of an expansion in a plane-wave basis, with a cutoff energy equal to 350 eV. The Monkhorst–Pack method with a $3 \times 1 \times 1$ network was used to generate k points [27]. Constancy of the total energy of the system (accurate to 10^{-5} eV) was a condition for the convergence of self-consistent calculations.

Since the calculations for moistened kaolinite samples are highly laborious, we used ab initio pseudopotentials [28], which take into account that the electrons of tightly bound filled electron shells of atoms barely change their state when interacting with other atoms. The parameters and models that we used make it possible to analyze fairly exactly the crystal structure and optical properties of minerals with spatial and electronic structures similar to the structure of the kaolinite under study [23].

When calculating the IR spectra of kaolinite, the crystallographic parameters listed in the table and characterizing the specific features of a material under study were taken as initial ones. During the self-consistent calculation, the structural parameters of kaolinite and H_2O molecules were refined with allowance for the specified sample humidity.

The electronic and spatial structures and the IR spectrum of kaolinite in the dry and moistened states were calculated using the exchange-correlation functional RPBE in the generalized gradient approximation (GGA), which proved to be good in calculating the electronic structure and properties of hydrogen-containing compounds [29, 30].

The dependence of the relative intensities of IR spectral lines on humidity was analyzed by the example of stretching vibration lines ν of the atoms belonging to the Si–O group. These lines were chosen because of their relatively high intensity and good resolution in the experiment. The corresponding fragment of the theoretical spectrum is compared with the experimental spectrum in Fig. 2. The shape of the theoretical spectrum was obtained by summing individual Gaussians, the areas of which was assumed to be equal to the intensities of individual vibrations. To perform a comparison with the experimental data, the energy of the theoretical spectrum was increased by 20 cm^{-1} and the FWHM value was chosen to be 25 cm^{-1}. This value somewhat exceeds the previously estimated width

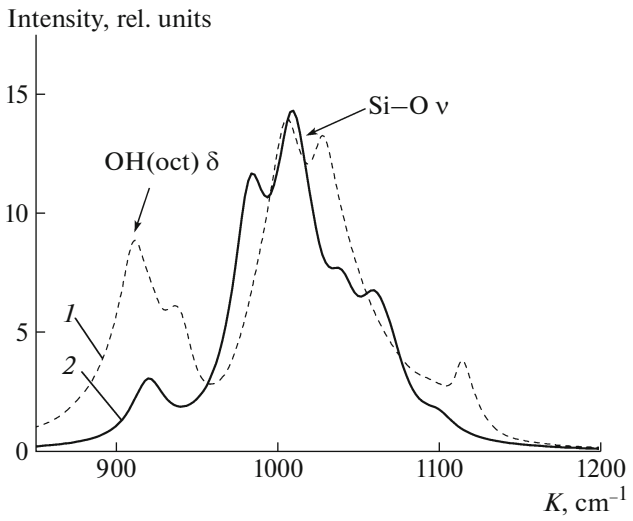

Fig. 2. IR spectrum of kaolinite in the air-dry state: experiment (*1*, dashed line) and theory (*2*, solid line). The fundamental spectral lines were identified according to [32].

(17.3 cm^{-1}) of the components of the IR spectrum of an association of clay minerals [31].

Analysis of the experimental and theoretical data in Fig. 2 indicates that the occurrence of absorption bands in the range of 850–1100 cm^{-1} is due to the stretching vibrations of the atoms belonging to the Si–O group and bending vibrations of the atoms of the O–H group on the hydroxyl surface. The strongest lines, with wavenumbers of 1007 and 1029 cm^{-1}, can also be assigned to these atoms. The bending vibrations of the OH groups of aluminum–oxygen octahedra of kaolinite manifest themselves in the range of 900–960 cm^{-1}.

Study of the Structure of H_2O Molecule

The structure of the H_2O molecule has been investigated fairly precisely, both experimentally and theoretically. Based on the experimental results of [33, 34], one can assume bond length r_{OH} and bond angle θ to be 0.958 Å and 104.5°, respectively; the errors of these values are smaller than the numbers in the last decimal place.

The theoretical analysis of the structural parameters of H_2O molecule was performed using different approaches: multiconfiguration approximation, consideration of the core and relativistic corrections, and application of an extended correlation set of basis functions. As a result, values coinciding with the aforementioned experimental data [35] were obtained for the structural characteristics under consideration.

The theoretical approaches based on the GGA RPBE approximation do not make it possible to calculate the structural parameters of the H_2O molecule with such a high accuracy. The calculations carried out for the H_2O molecule in the vapor phase yielded the

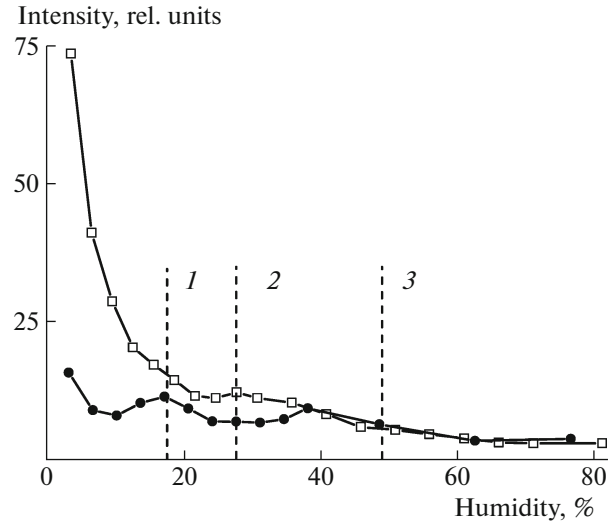

Fig. 3. Theoretical (filled circles) and experimental (open squares) dependences of the intensity of the Si–O stretching vibration lines ν from the siloxane surface on humidity, with indication of the humidity values at which (*1*) the formation of the first water layer on the grain surface is completed, (*2*) this layer is supplemented with bound water layers, and (*3*) and water layers are formed.

values for the O–H bond lengths and angles between these bonds of 0.965 Å and 104.3°, respectively. When the RPBE potential is used to calculate the H_2O in the liquid state, the corresponding parameters take values of 0.980 Å and 105.4°, respectively; we will use them in further analysis.

RESULTS AND DISCUSSION

The Influence of Humidity on the Intensity of Si–O Stretching Vibrations

The humidity of kaolinite with one H_2O molecule per unit cell (Fig. 1) is $w_1 = 3.49\%$. The theoretical spectra were calculated for a humidity of 76.78%, which corresponds to 22 H_2O molecules per unit cell. Figure 3 shows the intensity of the Si–O stretching vibration line (Fig. 2), normalized to the H_2O line intensity, as a function of the sample humidity. The experimental value of the wave number of Si–O stretching vibrations in the air-dry state of the sample is 1007 cm^{-1}. The line with a wave number of 1633 cm^{-1}, which was isolated at all humidity values, was used as the reference H_2O line.

A comparison of the above data shows that the behavior of the experimental and theoretical humidity dependences of the relative intensity of the line under consideration deviates from monotonic in the humidity range of 15–50%. This deviation can be explained by the end of the formation of surface bound water and the transition of the sample to the plastic state at $w = 15\%$.

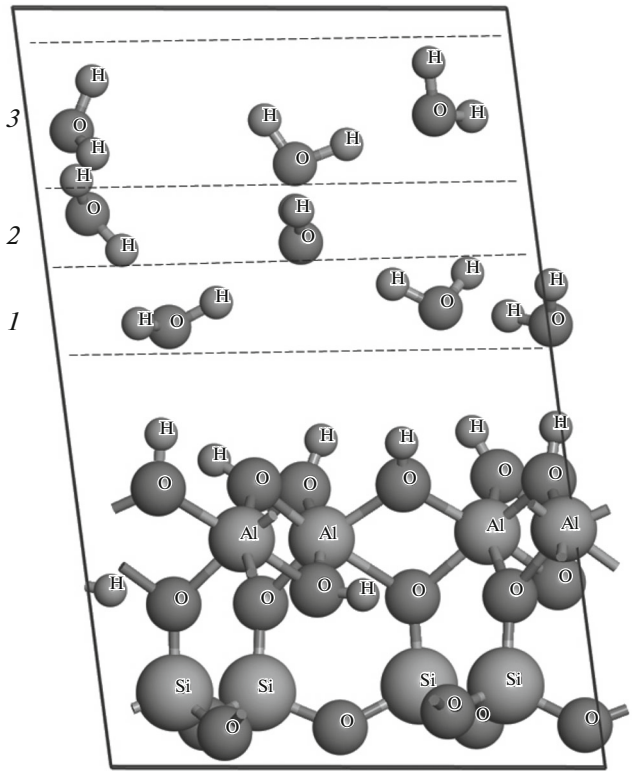

Fig. 4. Formation of surface-bound (sites *1* and *3*) and porous (site *2*) H_2O layers when the unit cell incorporates eight water molecules.

A calculation performed with optimization of the arrangement of kaolinite atoms and H_2O molecules made it possible to relate the singularities in the dependence of the intensity of Si–O stretching vibration line on humidity with the specific features of formation of water layers on kaolinite surfaces and in the porous space: the formation of the first water layer on the grain surface is completed at point *1*; at point *2*, this layer is supplemented with bound water layers, which facilitate mutual displacement of clay particles under an external impact; and the formation of water layers, providing the sample liquidity, is completed at point *3*.

Comparison of the data in Fig. 3 indicates that the theory describes well the experimental intensity ratio, beginning with 11 H_2O molecules per unit cell (humidity 38.4%). At this humidity, there are adsorbed H_2O layers in the volume between basal surfaces (2 or 3 molecules in a layer per unit cell), and the formation of a molecular layer is completed, which can be interpreted as water filling pores in the sample. The formation of porous water begins when the unit cell incorporates seven or eight H_2O molecules (Fig. 4).

The discrepancy between theory and experiment at lower water concentrations may be related to the insuf-

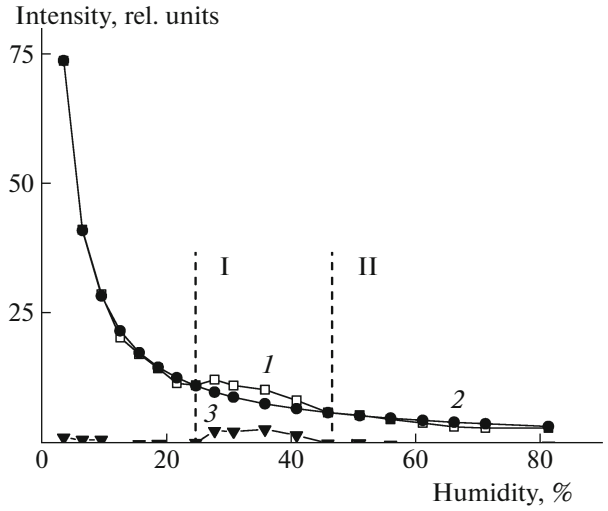

Fig. 5. (*1*) Experimental intensity of the Si–O stretching vibration line ν from the siloxane surface, (*2*) values of function $\Omega = Nm_{clay}/m_{H_2O}$, and (*3*) their difference.

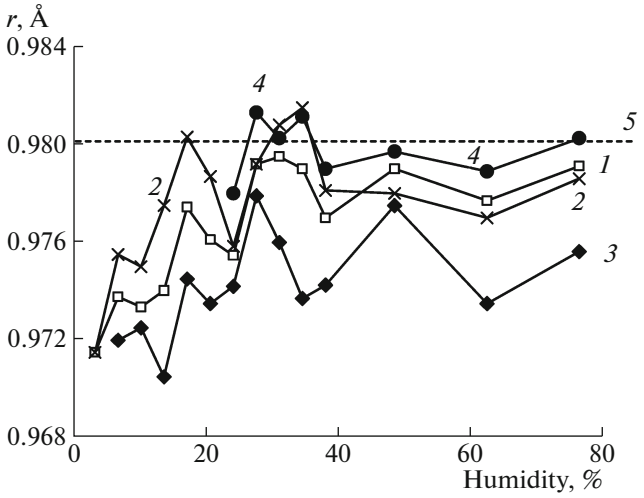

Fig. 6. Dependences of the average r_{OH} value on humidity (*1*) for all water molecules, (*2*) for water molecules at the hydroxyl surface, (*3*) at the siloxane surface, (*4*) in the porous space, and (*5*) in the liquid state.

ficiently accurate description of the spatial and electronic structures of the water molecules adsorbed by the basal surfaces of the mineral. The corresponding interactions and processes can be described more accurately by refining the DFT potentials, which is beyond the scope of this study.

Figure 5 shows the experimental intensity of the spectral line that is mainly due to the stretching vibrations of the Si–O atomic group and a function inversely proportional to the sample humidity, $\Omega = N/w$, where factor N is chosen so as to make the theory and experiment agree at point $w = 3.49\%$.

This figure also shows the difference between the experimental dependence and Ω, which is mainly localized between points I and II.

The humidity values at points I and II (25.4 and 46.1%, respectively) correlate well with the humidities at the plasticity (w_p) and liquidity (w_L) limits determined according to the existing regulatory documents [36–38]. For the kaolinite samples under study, they were found to be 27.3 and 47.0% [39]. Thus, analyzing the intensities of this spectral line, one can determine the aforementioned mechanical parameters of soils.

Specific Structural Features of the Water Molecules Interacting with Kaolinite Basal Surfaces

Figures 6 and 7 show the O–H bond lengths and H–O–H angles, averaged over water molecules and chemical bonds, as functions of the kaolinite humidity. The horizontal dashed lines indicate the values of these parameters calculated for the entire ensemble of H_2O molecules in the liquid state.

The observed nonsmoothness of the dependences may be related to specific features of implementing the numerical procedure. In addition, there may be an error caused by the separation (according to the calculation results) of water molecules into those adsorbed by basal surfaces and those localized in the porous space. At the same time, the difference in the parameters for the molecular configurations deviating by one water molecule does not exceed 1%.

It can be seen in Figs. 6 and 7 that an increase in humidity leads to convergence of the average values of parameters (*1*) and the parameters for the molecules in porous space (*4*) to the values found for water in the

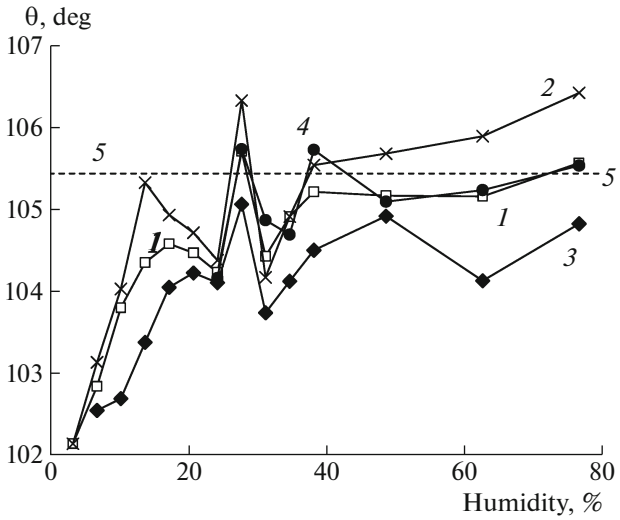

Fig. 7. Dependences of the average value of angle θ between OH bonds on humidity (*1*) for all water molecules, (*2*) for water molecules at the hydroxyl surface, (*3*) at the siloxane surface, (*4*) in the porous space, and (*5*) in the liquid state.

liquid state (*5*). The formation of porous water begins at a humidity exceeding 20% (six water molecules per unit cell).

In addition, the numerical values of the bond lengths and bond angles for the water molecules adsorbed by the hydroxyl surface are systematically larger than the corresponding values for the water molecules adsorbed by siloxane surfaces. When the first water molecule is introduced into the calculation model, the optimization of the position of the atoms of the system leads to its preferred localization near the hydroxyl surface of the mineral. This fact confirms the results of [17], where the high hydrophility of this kaolinite surface was theoretically substantiated. As compared with the free state of water, one can observe a significant decrease in the angle between the bonds and an increase in their length. A further increase in the number of water molecules in the calculation model leads to the formation of layers at basal surfaces; the layer at the hydroxyl surface is formed with an advance by one molecule as compared with the siloxane layer.

CONCLUSIONS

The behavior of the relative intensity of Si–O stretching vibration lines in the absorption spectrum of kaolinite was investigated as a function of its humidity. In the range within the humidity values corresponding to the plasticity ($w_P = 27.3\%$) and liquidity ($w_L = 47.0\%$) limits, where kaolinite exhibits plastic properties, the intensity of the above-considered line behaves anomalously. Thus, having determined the range of anomalous behavior of the intensity of this IR spectral line, one can find the range of plastic state of the mineral.

The water molecules adsorbed by basal kaolinite surfaces and the water molecules positioned in the porous space have different averaged O–H bond lengths and H–O–H angles. Our calculations showed that the bond lengths and bond angles for a water molecule adsorbed on a siloxane surface are systematically smaller than those for a water molecule adsorbed on a hydroxyl surface.

ACKNOWLEDGMENTS

This study was supported by the Ministry of Education and Science of the Russian Federation within grant agreement no. 14.607.21.0110 of November 27, 2014, unique identifier RFMEFI60714X0110.

REFERENCES

1. S. Pavlidou and C. D. Papaspyrides, Prog. Polym. Sci. **33**, 1119 (2008). doi 10.1016/j.progpolymsci.2008.07.008
2. E. I. Unuabonah and A. Taubert, Appl. Clay Sci. **99**, 83 (2014). doi 10.1016/j.clay.2014.06.016
3. A. Aznárez, R. Delaigle, P. Eloy, E. M. Gaigneaux, S. A. Korili, and A. Gil, Catal. Today **246**, 15 (2015). doi 10.1016/j.cattod.2014.07.024
4. L. F. B. L. Pontes, J. E. G. de Souza, A. Galembeck, and C. P. de Melo, Sens. Actuators B **177**, 1115 (2013). doi 10.1016/j.snb.2012.12.001
5. D. Plachá, K. Rosenbergová, J. Slabotínský, K. Mamulová Kutláková, S. Študentová, and G. Simha Martynková, J. Hazard. Mater. **271**, 65 (2014). doi 10.1016/j.jhazmat.2014.01.059
6. P. Landais and J.-F. Aranyossy, Phys. Chem. Earth, Pt. A/B/C **36**, 1437 (2011). doi 10.1016/j.pce.2011.11.002
7. M. Dondi, M. Raimondo, and C. Zanelli, Appl. Clay Sci. **96**, 91 (2014). doi 10.1016/j.clay.2014.01.013
8. F. Bergaya, B. K. G. Theng, and G. Lagaly, *Handbook of Clay Science* (Elsevier Science, Amsterdam, 2006).
9. P. Hohenberg and W. Kohn, Phys. Rev. B **136**, 864 (1964). doi doi 10.1103/PhysRev.136.B864
10. W. Kohn and L. J. Sham, Phys. Rev. A **140**, 1133 (1965). doi 10.1103/PhysRev.140.A1133
11. J. Ortega-Castro, N. Hernández-Haro, D. Muñoz-Santiburcio, A. Hernández-Laguna, and C. I. Sainz-Díaz, J. Mol. Struct.: THEOCHEM **912**, 82 (2009). doi 10.1016/j.theochem.2009.02.013
12. E. Scholtzováa, D. Tunegab, J. Madejováa, H. Pálkováa, and P. Komadela, Vibrat. Spectrosc. **66**, 123 (2013). doi 10.1016/j.vibspec.2013.02.006
13. M.-C. He, J. Zhao, and S.-X. Wang, Appl. Clay Sci. **85**, 74 (2013). doi 10.1016/j.clay.2013.08.045
14. V. Timóna, C. S. Praveen, E. Escamilla-Roa, and M. Valant, J. Mol. Graph. Model. **44**, 129 (2013). doi 10.1016/j.jmgm.2013.05.005
15. T. D. K. Wungua, F. Rusydi, H. K. Dipojono, and H. Kasai, Solid State Commun. **152**, 1862 (2012). doi 10.1016/j.ssc.2012.06.020
16. C. Zhang, Y.-H. Qi, P. Qian, M.-J. Zhong, L. Wang, and H.-Z. Yin, Comp. Theor. Chem. **1046**, 10 (2014). doi 10.1016/j.comptc.2014.07.004
17. R. Šolc, M. H. Gerzabek, H. Lischka, and D. Tunega, Geoderma **169**, 47 (2011). doi 10.1016/j.geoderma.2011.02.004
18. X. L. Hu and A. Michaelides, Surf. Sci. **601**, 5378 (2007). doi 10.1016/j.susc.2007.09.012
19. X. Liu, X. Lu, R. Wang, E. Jan Meijer, H. Zhou, and H. He, Geochim. Cosmochim. Acta **92**, 233 (2012). doi 10.1016/j.gca.2012.06.008
20. F. Bergaya and G. Lagaly, *Handbook of Clay Science* (Elsevier Science, Amsterdam, 2013).
21. G. S. Berger and I. A. Efimov, *Methods of Separation of Monomineral Fractions* (Gosgeoltekhizdat, Moscow, 1963) [in Russian].
22. ISO 13318-1:2001. Determination of particle size distribution by centrifugal liquid sedimentation methods.
23. V. A. Yavna, A. S. Kasprzhitsky, and G. I. Lazorenko, in *Advanced Nano- and Piezoelectric Materials and Their Applications,* Ed. by I. A. Parinov (Nova Science, New York, 2014).
24. D. L. Bish, Clay Clay Miner. **37**, 289 (1989). doi 10.1346/CCMN.1989.0370401
25. D. L. Bish, Clay Clay Miner. **41**, 738 (1993). doi 10.1346/CCMN.1993.0410613

26. V. Sadovnichy, A. Tikhonravov, Vl. Voevodin, and V. Opanasenko, in *Contemporary High Performance Computing: From Petascale toward Exascale,* Chapman Hall/CRC Computational Science (CRC, Boca Raton, 2013).

27. H. J. Monkhorst and J. D. Pack, Phys. Rev. B **13**, 5188 (1976). doi 10.1103/PhysRevB.13.5188

28. D. R. Hamann, M. Schluter, and C. Chiang, Phys. Rev. Lett. **43**, 1494 (1979). doi 10.1103/PhysRevLett.43.1494

29. M. Ni and Z. Zeng, J. Mol. Struct.: THEOCHEM **910**, 14 (2009). doi 10.1016/j.theochem.2009.06.008

30. V. Verdinelli, E. German, P. Jasen, E. González, and J. M. Marchetti, Int. J. Hydrogen Energy **39**, 8621 (2014). doi 10.1016/j.ijhydene.2013.12.072

31. V. A. Yavna, A. S. Kasprzhitskii, G. I. Lazorenko, and A. G. Kochur, Opt. Spectrosc. **118**, 529 (2015). doi 10.1134/S0030400X15040220

32. J. Madejova and P. Komadel, Clay. Clay Miner. **49**, 410 (2001). doi 10.1346/CCMN.2001.0490508

33. W. S. Benedict, N. Gailar, and E. K. Plyler, J. Chem. Phys. **24**, 1139 (1956).

34. F. C. de Lucia, P. Helminger, R. L. Cook, and W. Gordy, Phys. Rev. A **5**, 487 (1972). doi 10.1103/PhysRevA.5.487

35. O. L. Polyansky, A. G. Csaszar, S. V. Shirin, N. F. Zobov, P. Barletta, J. Tennyson, D. W. Schwenke, and P. J. Knowles, Science **299**, 539 (2003). doi 10.1126/science.1079558

36. GOST (State Standard) No. 5180-84. Soils. Laboratory determination methods of physical parameters.

37. ISO/TS 17892-12:2004. Geotechnical investigation and testing—Laboratory testing of soil. Part 12: Determination of the Atterberg limits.

38. ASTM D 4318-10. Standard test method for liquid limit, plastic limit, and plasticity index of soil.

39. G. I. Lazorenko, A. S. Kasprzhitskii, and V. A. Yavna, Kondens. Sredy Mezhfaz. Granitsy **16**, 479 (2014).

Translated by Yu. Sin'kov